46th AIAA/ASME/ASCE/AHS/ASC Structures, Structural Dynamics & Material Conference, Austin, TX, April 18-21, 2005

PAPER AIAA-2005-2148

Computational Advances in Reliability Assessment of Aircraft Structures Under Corrosion-Fatigue Damage

Dr. Dan M. Ghiocel and Dr. Letian Wang*
Ghiocel Predictive Technologies, Inc.
6 South Main St., 2nd Floor, Pittsford NY, 14534, USA
**Email: dan.ghiocel@ghiocel-tech.com*
Http://www.ghiocel-tech.com

Abstract

The paper illustrates how probabilistic physics-based models can be used for risk-based condition assessment and life prediction of aircraft components including the uncertainties in maintenance activities. Although this paper focuses on aircraft components subjected to corrosion-fatigue damage, the proposed approach can be extended elsewhere to any mechanical system or component under progressive damage. Probabilistic modeling includes all significant uncertainties that affect aircraft component reliability, such as flight conditions, operational loading and environmental severity, manufacturing deviations, material properties and maintenance inspection activities. Advanced response surface modeling tools based on stochastic field approximation models were employed for computing the local bivariate stochastic stresses (mean stress and stress range are the two correlated stress components). Maintenance uncertainties related to the NDI techniques and operator's skills were also included in the reliability analysis. To do the life and risk computations the ProCORFA software was employed. This software was developed by Ghiocel Predictive Technologies in collaboration with STI Technologies for the US Air Force.

1.0 Introduction

A continuing challenge in the aviation industry is how to safely keep aircraft in service longer with limited maintenance budgets. Probabilistic methods provide tools to better assess the impact of uncertainties on component life and risk of failure. Probabilistic tools applied to risk-based condition assessment and life prediction help managers to make better risk-informed decisions regarding aircraft fleet operation and airworthiness. In addition to assessing aircraft reliability, probabilistic methods also provide information for performing an analysis of the cost of continuing operation based on risks and their financial consequence.

Corrosion and fatigue, separately or in combination, are serious threats to the continued safe operation of aircraft. As a result, the US Air Force, the US Navy, the FAA and the JAA have guidelines on how aircraft should be designed and maintained to minimize the risk of failure from fatigue damage.

Aircraft structure joints are the most fatigue and corrosion susceptible areas on an aircraft. Loads are transferred from one structural detail to another through fasteners with the attendant stress-concentrating holes making this a prime location for fatigue cracks to form. The tight fit of details and fasteners can trap moisture in the joint. Relative movement between the structural details and the fasteners, as well as the stress concentrations, can cause corrosion protection systems (anodize, primer and topcoat) to crack and wear allowing moisture to reach the aluminum parts and start the corrosion process.

This paper presents an illustrative reliability analysis of an aircraft structure joint under corrosion-fatigue progressive damage. The computational reliability analyses were performed using the ProCORFA software developed by GP Technologies in collaboration with STI Technologies for USAF.

Copyright 2005 by the American Institute of Aeronautics and Astronautics, Inc. All rights reserved.

2.0 Aircraft Lapjoint Example

The investigated example aircraft structure joint is a longitudinal skin joint on the pressurized fuselage of a transport aircraft (Figure 1). The loading of longitudinal skin joints, particularly those on or near the horizontal neutral axis of the fuselage, is simply the pressurization of the fuselage, which is approximately constant amplitude with a stress ratio (ratio between minimum over maximum stress) of zero. For illustration purposes, we assume that there is only a single pressurization stress cycle per flight.

To keep the discussion simple, the illustrative examples presented in this section include only the effect of pitting corrosion of corrosion-fatigue life. The effects of other corrosion types, including intergranular corrosion in early stages, or general thickness loss and pillowing in later stages are not considered. No cladding was assumed. Also, the multiple site damage (MSD) or widespread fatigue damage (WFD) that usually produces the ultimate lapjoint system failures are not included. Only the local failure in critical locations is considered. However, both MSD and WFD are real threats to aircraft structural integrity and therefore they must be considered when evaluating the risk of failure for an actual aircraft structure.

The major loading in the lapjoint comes from the pressurization in the aircraft. The input random variables included in the probabilistic life analysis are shown in Table 1. The input random variables related to manufacturing are given in Table 2.

Figure 2 illustrates the stochastic history of pressure loading and environmental conditions of the aircraft. The elementary constituent of the stochastic history of the lapjoint is the block that includes a single flight and a single stay on ground. It was assumed that the random pressure load is described by a single cycle for each flight. The environmental severity condition that drives corrosion was considered to randomly vary with the airport location. However, for the same location it was assumed that the environmental condition is a time-invariant quantity. The surface particles (that are initial discontinuity states) were assumed to be the initiators of corrosion pits and fatigue micro-cracks. The environmental severity condition characterized by the pit growth rate was modeled by a highly skewed probability distribution. A truncated exponential distribution was used to fit the trend of the measured corrosion rate data at different airport locations. These large differences in values indicate that the crevice pits can grow up to ten times faster in some airport locations than in others.

Hierarchical, Multi-Scale Stochastic FE Analysis

A three-level hierarchical, multi-scale, stochastic FE analysis approach was employed for computing stochastic local stresses. The employed three-level hierarchical stochastic FE analysis is capable of computing accurately the stochastic stresses variations near rivets that are caused by loading, material, geometric configuration uncertainties, including deviations from the baseline geometry of the lapjoint due to manufacturing process.

At the top level, a global airframe FE model with a relative coarse mesh was used. At an intermediate level, a local FE model of the lapjoint was used. The computed displacement response of the global FE model was considered to be the input boundary conditions for the local FE analysis of the lapjoint. This local FE model included the joint rivets and splices, plus the contact surface conditions between the joint components as shown in Figure 4. At the bottom level, a very local axisymmetric FE model of a single rivet was employed. This detailed single rivet FE model has a very refined mesh that was required for incorporating accurately material plasticity effects on the local contact stresses around the rivet. Thus, using this rivet FE model the residual stresses that are caused by the cold work were computed.

Cold work process is usually applied to the rivet hole before assembling. The residual compressive stresses created by cold works are beneficial to the fatigue life extension. The effect of residual stresses is to lower the mean stress life reduction effects. The residual stresses were computed using a three step procedure:

Copyright 2005 by the American Institute of Aeronautics and Astronautics, Inc. All rights reserved.

Step 1: Apply rivet interference and perform a contact elasto-plastic analysis.
Step 2: Remove rivet and then apply the displacements computed from contact elasto-plastic analysis to perform another nonlinear material analysis without contact. This model is an equivalent with the model used in Step 1 except that the contact elements were eliminated.
Step 3: Release the displacement constraints and then perform another nonlinear material analysis to get the residual stresses and strains around the rivet.

Probabilistic stress response sensitivity study was performed by comparing the local stress response computed for all input random variables with the local stress response computed for all input variables minus one variable, as shown in Table 3. From Table 3, it should be noted that the stochastic local stresses are most sensitive to rivet interference variable. The plate thickness variable has also a significant influence on local stochastic stresses, on both mean and standard deviation of the local stress. The corrosion material loss and the hole location variables affect mostly the standard deviation of local stresses.

Simulation of Stochastic Corrosion Surface Topography

Stochastic corrosion topography surfaces were simulated using the Karhunen-Loeve expansion (Ghiocel, 2001, 2005) as shown in Figure 5. The FE mesh of the lapjoint including the corrosion material loss is shown in Figure 6. The gaps produced by corrosion between rivet and splices, and between the layered splices are highly visible in the figure.

Comparison of Results with Corrosion and Without Corrosion

The local stress responses are compared in Table 4. The main effect of corrosion is to shift the mean stress value by 2ksi to a higher value, and to increase the standard deviations to 19% and 39% for the stress range and the mean stress, respectively.

Stochastic Response Approximation

To reduce the computational effort of the stochastic FE analysis of the aircraft lapjoint, an advanced response surface modeling was used. Only a reduced number of FE calculations, as low as 125, were needed for building refined response surface models for the 8D stochastic FE lapjoint analysis.

To verify the accuracy of response model, we compared the response surface solutions with direct FE analysis solutions. The relative errors were less than 2% for the most critical locations, Hole 1, Location 3 (see Figure 3).

The stochastic local stress at critical locations is a bivariate stochastic quantity that includes the stress range component and the mean stress component, respectively. Figure 7 shows the bivariate histogram and the bivariate PDF of the local stress at the Hole #1 Location 3. The bivariate stress PDF was obtained by smoothing the bivariate histogram estimate with a 2D Parzen moving window.

Figure 8 shows the conditional response surface at Hole #3 Location 7 in two dimensions. We considered the random interference of Hole #1 and the random thickness change of Plate #1 and other six as fixed value. It shows that the stress response is influenced by both random variables.

Flight Scenarios

Four flight scenarios were investigated for reliability analysis of the aircraft lapjoint [1]. The four scenarios were obtained by combining to two aircraft operating scenarios, namely (i) one flight /day and (ii) three flights/day with two flying scenarios, namely (i) each aircraft flies from an airport location to the same airport location - without random rotation of the airport location - and (ii) each aircraft flies randomly from an airport location to any other airport location - with random rotation of the airport location. In the last flying scenario it was assumed that all airport locations are equally probable and each individual aircraft can visit all airport locations. This is the ideal situation for reducing corrosion effect scatter assuming a uniform distribution of the aircraft fleet across the airport location set.

To compute the probabilistic corrosion-fatigue life of the lapjoint both the crack initiation and

Copyright 2005 by the American Institute of Aeronautics and Astronautics, Inc. All rights reserved.

the crack propagation stages were included. The stochastic strain-life curve and the stochastic Forman crack propagation models were developed from the deterministic models based on the assumption that their parameters are random quantities as shown in Table 1. To include the effect of pitting corrosion on the lapjoint fatigue life a simultaneous corrosion-fatigue (SCF) model was employed [1].

Figure 9 shows the simulated pit depth growth curves for all airport locations assuming no rotation of airport locations. These pit curves were computed using Wei pitting model [2]. The pit growth curves shown in the figures stop at the failure times. Figure 3 includes both the one-flight/day scenario and and the three-flights/day scenario, respectively. Figure 4 shows the pit growth curves for the same two scenarios with a random rotation of aircraft location. It was assumed that each aircraft has an equal probability to fly to any airport location. This means there is a high probability that each airport will be visited about the same number of times by each aircraft. Therefore, for the scenario with the airport rotation, the scatter of the pit growth drops significantly converging in the limit to the (deterministic) mean pit growth for an infinite number of flights per aircraft.

Computed Results

The computed corrosion-fatigue life histograms (with different incremental steps) for the assumed four cases are shown in Figure 10. It should be noted that the mean corrosion-fatigue life is about double for the one-flight/day scenario versus three-flights/day scenario. Figure 11 illustrates the probability density of the time until a 5.0 mm crack length is reached for the one-flight/day scenario, without airport rotation and with airport rotation, respectively. The computed probability densities (PDF) are compared with analytical densities, namely the lognormal and normal probability densities. It should be noted that for the without rotation case, the computed skewed density is far from the lognormal density, while for the with rotation case, the computed density is very close to normal density. For the former case, without rotation, the heavy right tail of the PDF shape is due to the fact that many airport locations have milder environmental severity conditions. For the latter case, the scatter of corrosion effects is reduced and the probability density converges to the normal distribution in accordance with the central limit theorem.

To consider the effect of maintenance, the uncertainties associated with the probability of crack detection for different standard NDE inspections were included using the appropriate POD curves. The Eddy Current NDE technique with different operator skill classes was considered. The Eddy Current POD curve was assumed to correspond to a lognormal distribution with a logarithmic mean and logarithmic standard deviation of (i) -4.73 and 0.98 for the best operator, (ii) –3.75 and 0.70 for the average operator and (iii) for –2.73 and 0.45 for the worst operator. No crack sizing error was included in addition to operator's skill variation. At each inspection time, the statistical crack population was filtered through the POD curve. Based on the computed probabilities of acceptance or rejection, each crack was randomly accepted or removed by replacing the cracked component. The repair effects were not considered for this illustrative example.

Figures 12 and 13 indicate the inspection schedule required over 20,000 days (about 60 years) for maintaining the corrosion-fatigue damage risk under a reliability target defined by a upper bound failure probability of $2x10^{-7}$. Figure 12 shows the results computed for the one-flight/day scenario without airport rotation. Figure 12 compares results for different NDE operator's skills (best operator versus worst operator) and for different failure limit criteria (crack limit of 1.0 in versus crack limit of 0.40 in). It should be noted that the minimum inspection interval drops from 2,300 days (6,450 FH) to 1,300 days (3,640 FH) due to the NDE operator's skill, and from 2,300 days (6,540 FH) to 900 days (2,520 FH) due to the crack limit criterion considered.

Figure 13 compares the required inspection schedules for the two cases, without and with airport rotation, including both the one-flight/day

Copyright 2005 by the American Institute of Aeronautics and Astronautics, Inc. All rights reserved.

scenario and three-flights/day scenario, assuming the same reliability target, an average operator's skill and a 1.0 in crack limit failure criterion. Without the airport rotation, the required inspection intervals in real time are about two-three times longer for the one-flight/day scenario than for the three-flights/day scenario. However, if the inspection intervals are measured in effective FH instead of days, this observation is not true. The minimum inspection intervals are 1,600 days (4,480 FH) for the one-flight/day scenario and 600 days (5,040 FH) for the three-flights/day scenario. The increase of the inspection intervals expressed in flight hours from the one-flight/day scenario to three-flights/day scenario indicates that the effects of corrosion are more severe for one-flight/day when the time spent by an aircraft on ground is longer. With the airport rotation, the minimum inspection intervals are much longer than those computed without airport location rotation. The minimum inspection intervals are 11,200 days (31,360 FH) for the one-flight/day scenario and 4,600 days (38,640 FH) for the three-flights/day scenario. This large benefit effect of the random rotation of airport locations is mainly a result of the large reduction is the statistical scatter of corrosion effects as a result of the central limit theorem.

The exclusive use of *instantaneous* failure probabilities to characterize aircraft reliability is insufficient for setting the risk-based maintenance strategy. This is because from a risk-based maintenance point of view, one is interested in the aircraft reliability over a period of time, not only at the critical instantaneous times. To illustrate the point, we can review the results in Figure 13. For the inspection schedule shown, the maximum risk is almost constant with a value of 1.2×10^{-7}. The maximum risk is bounded to 1.2×10^{-7} independent of the aircraft operating scenarios, without or with airport location rotation.

However, the number of inspections is different, so that number of times when the maximum failure risk is reached is different for the two operating scenarios. Thus, if the average hazard failure rates over a long period are computed they are very different.

For the results in Figure 13, if the average hazard failure rates are computed over the 20,000 days (about 60 years) period, these are 1.04×10^{-10} event/day and 7.97×10^{-12} for the case without airport rotation and the case with rotation, respectively.

3.0 Concluding Remarks

Computational risk-based maintenance using physics-based stochastic damage models, carefully calibrated with appropriate empirical data, provides a quantitative process for simultaneously maximizing aircraft availability and reducing maintenance costs while maintaining safety and airworthiness. The physics-based stochastic modeling tools and computational reliability methods are sufficiently mature for solving the aircraft fleet reliability – based maintenance problem based on a full probabilistic approach.

4.0 Acknowledgments

The authors acknowledge Dr. Eric Tuegel, AFRL, Air Vehicle Directorate, and Dr. Craig Brooks, APES Inc. for their valuable technical advices on many issues related to this paper.

5.0 References

1. Ghiocel, D.M. and Tuegel, E.J. "Reliability Assessment of Aircraft Structure Joints Under Corrosion-Fatigue Damage", Chapter in CRC "Engineering Design Reliability Handbook", Eds. E. Nikolaidis, D.M. Ghiocel and S. Singhal, CRC Press, December, 2004

2. Ghiocel, D.M.,"Advances in Computational Risk Predictions for Complex, Large-Size Applications, 46th AIAA SDM Conference, Paper AIAA-2005-2222, Austin, TX, April, 2005

3. Wei, R.P.,"Corrosion and Corrosion Fatigue ofAirframe Materials", FAA report DOT/FAA/AR-00/22, 2000

Copyright 2005 by the American Institute of Aeronautics and Astronautics, Inc. All rights reserved.

Table 1. Stochastic Parameters for Loading and Material

Random Parameter	Mean	Standard Deviation	Probability Distribution
Uniform Pressure Inside Aircraft, p	59.3 Pa	2.97 Pa	Normal
Single Flight Duration, d	2.8 hours	0.50 hours	Lognormal
Surface Particle Size, a_0	13.66 microns	6.02 microns	Weibull
Strain Life Curve Exponent, b and c	-0.114, -0.927	0.00114, 0.00927	Normal, Normal
Strain Life Curve Parameters, σ_f' and ε_f'	1044MPa 1.765	20.88MPa 0.0353	Normal Normal
Stress Intensity Range Threshold, ΔK_{th}	3.00 MPa$\sqrt{m}$	0.15 MPa$\sqrt{m}$	Normal
Toughness, K_c	97.7 MPa$\sqrt{m}$	2.93 MPa$\sqrt{m}$	Normal
Pit Growth Parameter, I_{PO}, in Wei Model Variation due to the Environmental Conditions at Different Airport Locations	14.08 C/s	22.26 C/s	Truncated Exponential, from 0.1 and 100 C/s

Table 2. Stochastic Variations due to Manufacturing Deviations

Variables Description	Distribution	Mean	Standard Derivation
Change of plate thickness (inch)	Normal	0.0	0.001
Rivet hole expansion (inch)	Log Normal	0.00393	0.00208
Change of hole location (inch)	Normal	0.0	0.0033
Interference (inch, in diameter)	Normal	0.001	0.0003

Table 3. Probabilistic Stress Response Sensitivities for Aircraft Lap Joint

Cases	Location at rivet holes	Stress Range (ksi)				Mean Stress (ksi)			
		Mean		Standard derivation		Mean		Standard derivation	
		Value	Sensitivity	Value	Sensitivity	Value	Sensitivity	Value	Sensitivity
Consider all random variables	L3 Hole 1	61.231	0.0%	3.203	0.0%	36.652	0.0%	1.016	0.0%
	L7 Hole 3	21.176	0.0%	3.574	0.0%	41.988	0.0%	7.697	0.0%
Consider Corrosion *	L3 Hole 1	61.758	0.9%	3.605	12.6%	38.615	5.4%	1.417	39.5%
	L7 Hole 3	21.533	1.7%	4.252	19.0 %	43.807	4.3%	7.983	3.7%
Exclude Interference	L3 Hole 1	70.779	-13.5%	1.234	159.6%	35.39	3.6%	0.617	64.7%
	L7 Hole 3	57.187	-63.0%	1.433	149.4%	28.593	46.8%	0.717	973.5%
Exclude hole diameter changes	L3 Hole 1	60.645	1.0%	3.037	5.5%	36.416	0.6%	1.013	0.3%
	L7 Hole 3	21.284	-0.5%	3.578	-0.1%	42.522	-1.3%	7.834	-1.7%
Exclude hole location shift	L3 Hole 1	61.216	0.0%	2.97	7.8%	36.648	0.0%	0.862	17.9%
	L7 Hole 3	21.184	0.0%	3.566	0.2%	41.994	0.0%	7.696	0.0%
Exclude plate thickness changes	L3 Hole 1	65.626	-6.7%	2.655	20.6%	34.447	6.4%	1.248	-18.6%
	L7 Hole 3	46.822	-54.8%	12.664	-71.8%	29.142	44.1%	7.168	7.4%

Copyright 2005 by the American Institute of Aeronautics and Astronautics, Inc. All rights reserved.

Table 4. Effect of Corrosion Material Loss on Stress Range and Mean Stresses

Cases	Location at rivet holes	Stress Range (ksi)				Mean Stress (ksi)			
		Mean		Standard derivation		Mean		Standard derivation	
		Value	Change	Value	Change	Value	Change	Value	Change
No corrosion	L3 Hole 1	61.231	0.0%	3.203	0.0%	36.652	0.0%	1.016	0.0%
	L7 Hole 3	21.176	0.0%	3.574	0.0%	41.988	0.0%	7.697	0.0%
Consider Corrosion	L3 Hole 1	61.758	0.9%	3.605	12.6%	38.615	5.4%	1.417	39.5%
	L7 Hole 3	21.533	1.7%	4.252	19.0 %	43.807	4.3%	7.983	3.7%

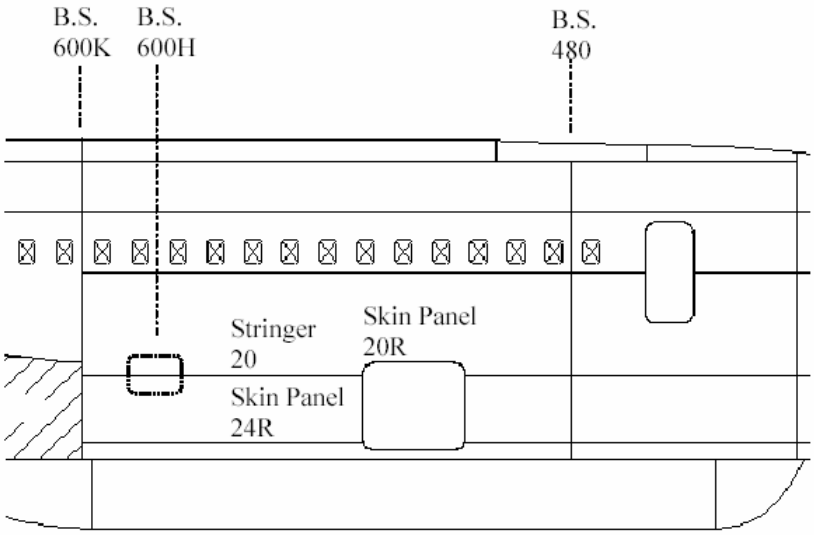

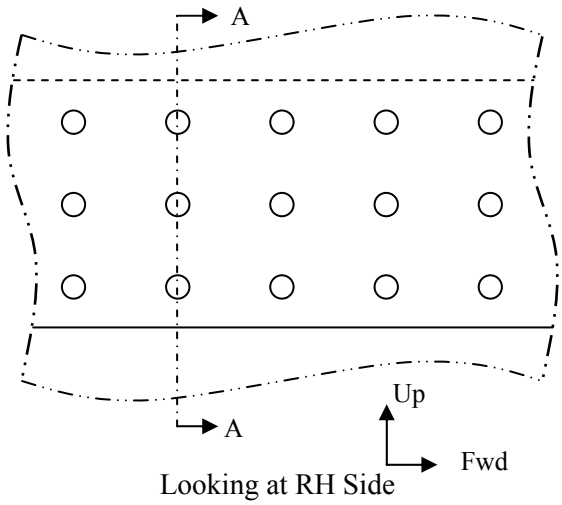

- Material: 2024-T3 Clad
- Max. σ = 94.05 MPa
- Thru stress ratio = 0.658
- Bearing stress ratio = 1.79

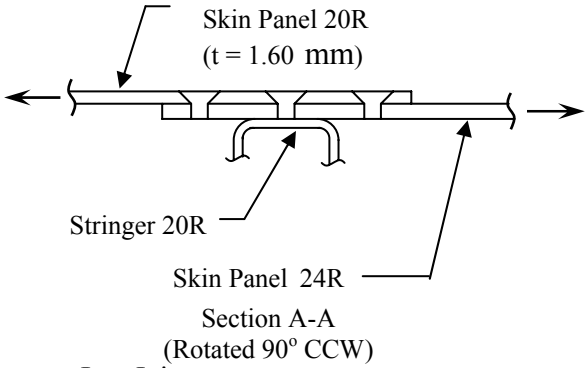

- Rivet diameter = 4.85 mm
- Rivet spacing = 25.4 mm

Figure 1. Details of Aircraft Structure Lap Joint

Copyright 2005 by the American Institute of Aeronautics and Astronautics, Inc. All rights reserved.

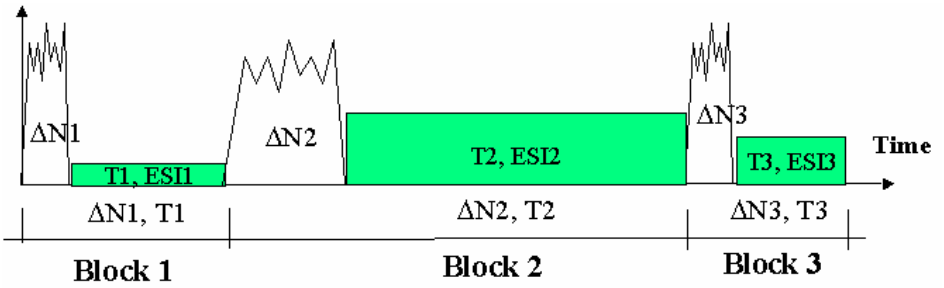

Figure 2. Stochastic History of Loading and Environmental Conditions

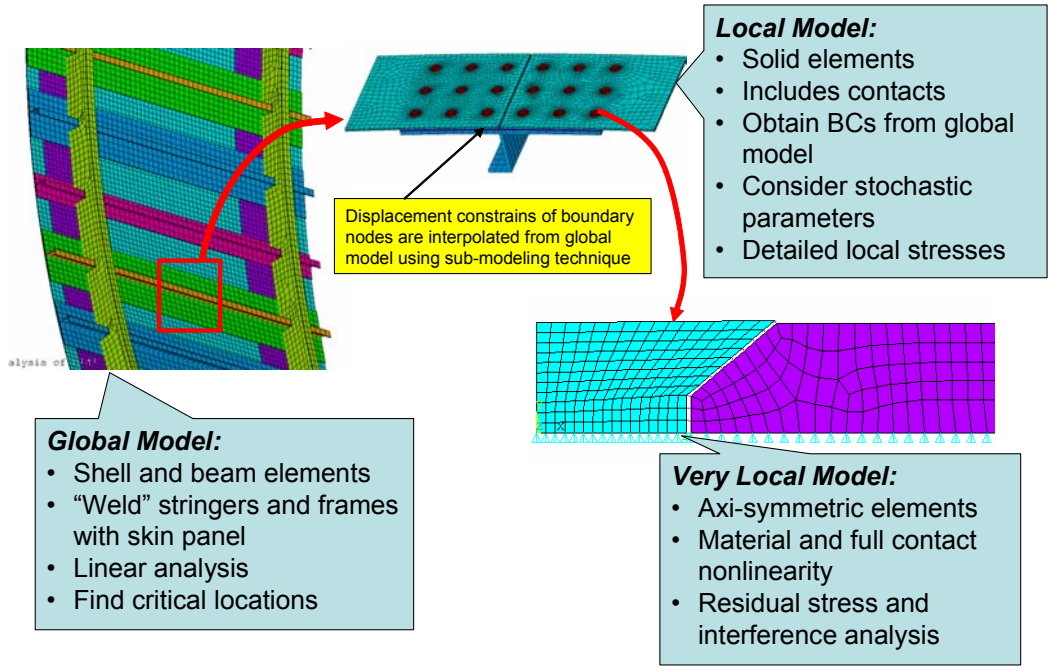

Figure 3. Three-Level Hierarchical, Multi-Scale Stochastic FE Analysis of Aircraft Structural Joints

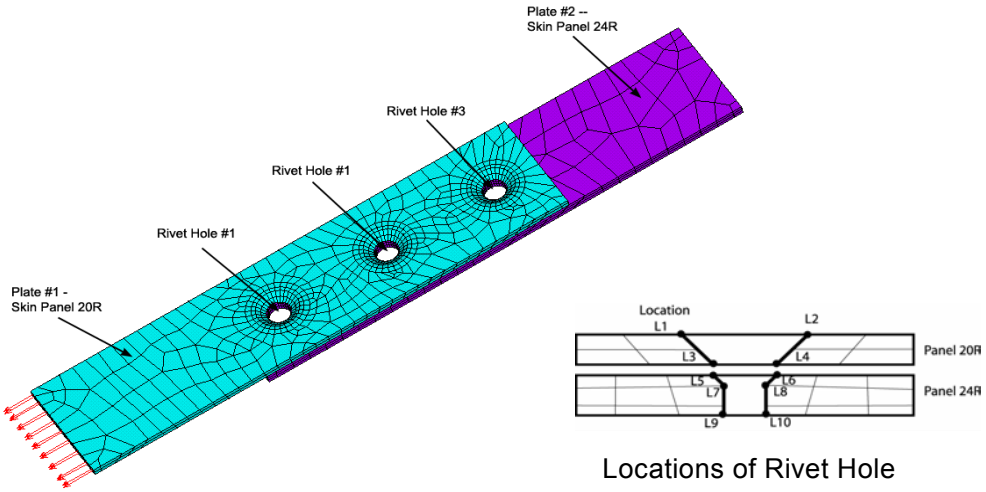

Figure 4. Identified Critical Stress Locations Around the Rivets

Copyright 2005 by the American Institute of Aeronautics and Astronautics, Inc. All rights reserved.

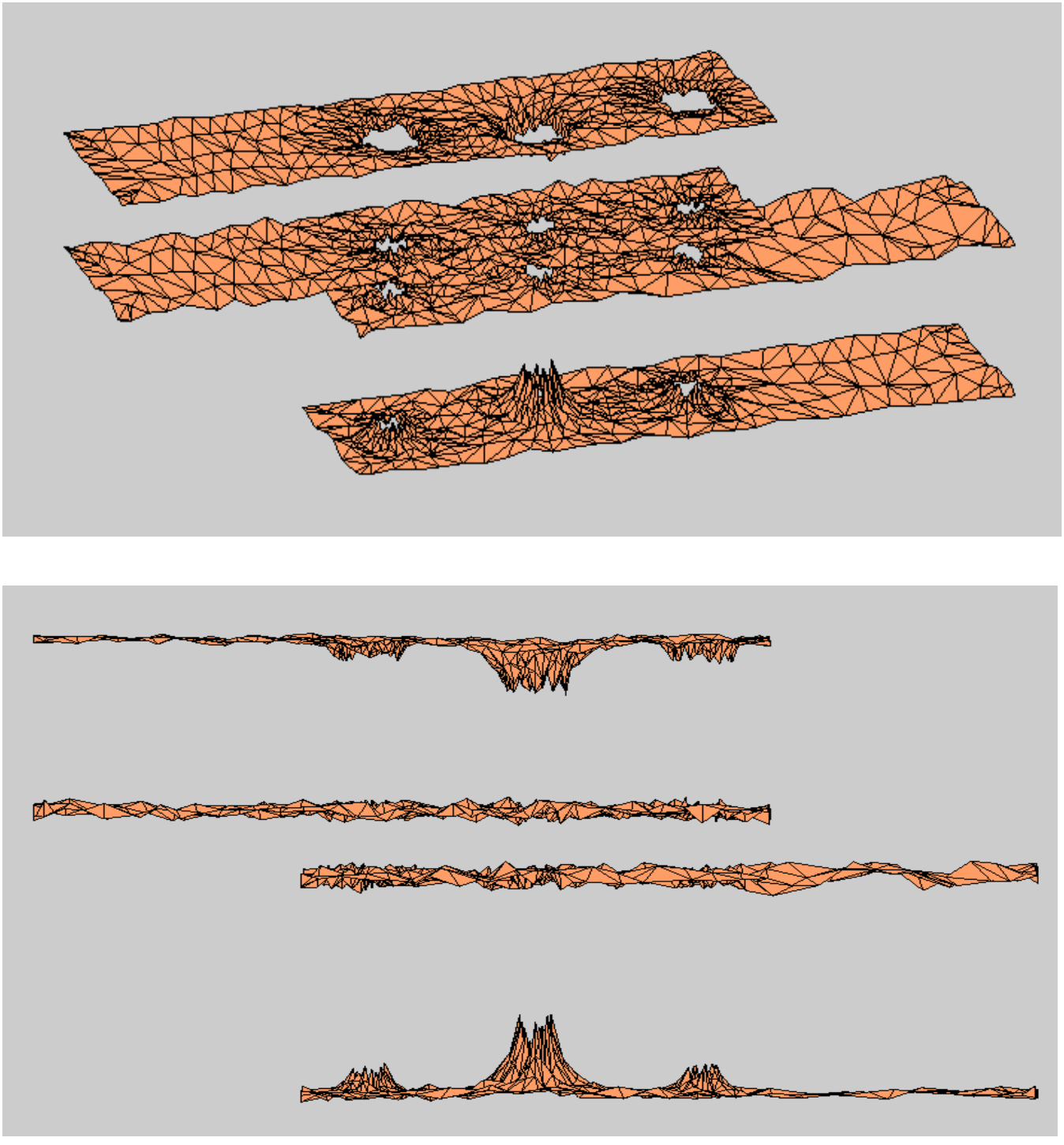

Figure 5. Simulated Stochastic Corroded Surface Topography

Copyright 2005 by the American Institute of Aeronautics and Astronautics, Inc. All rights reserved.

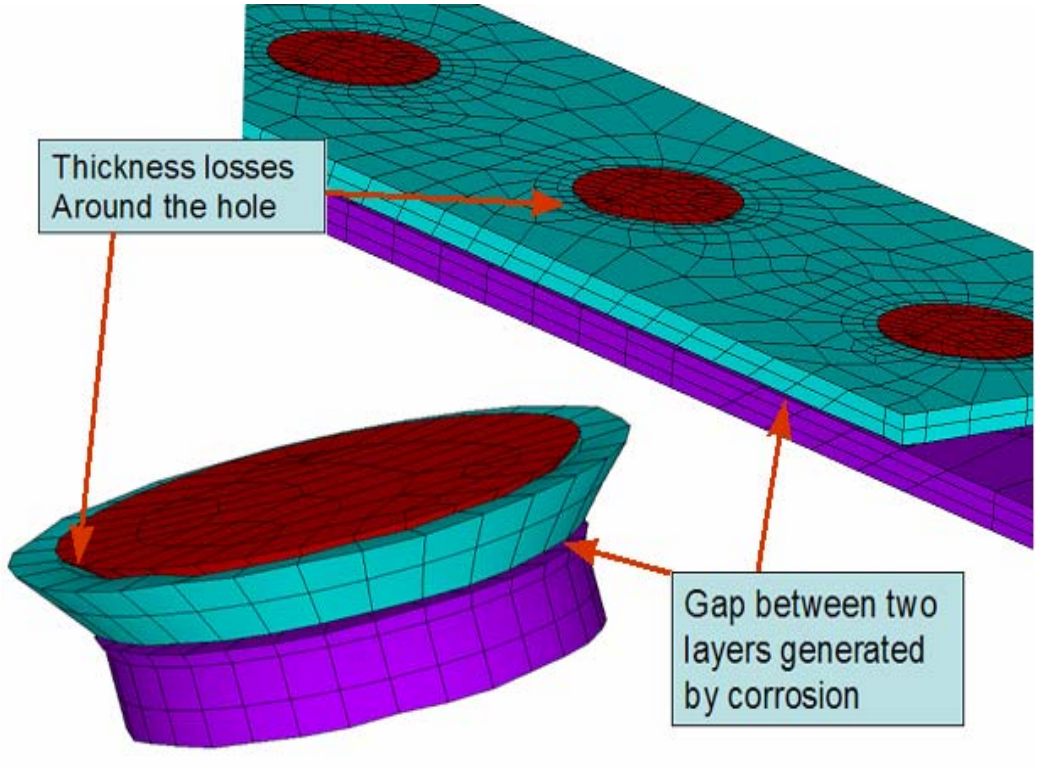

Figure 6. Stochastic FE Model Including Material Loss due to Corrosion Effects

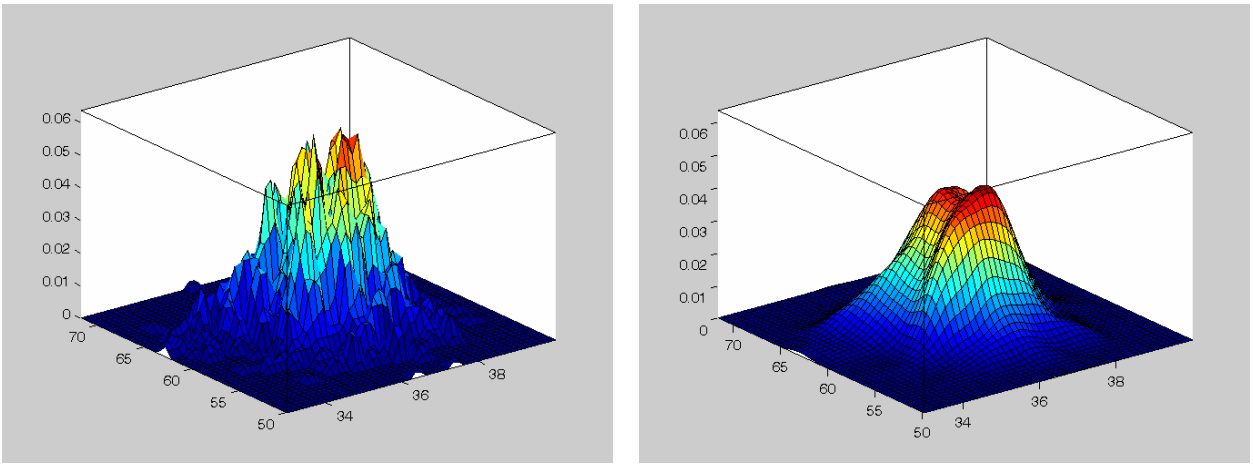

Figure 7. Histogram vs. Bivariate PDF for Stress Range and Mean Stress at the Critical Location

Copyright 2005 by the American Institute of Aeronautics and Astronautics, Inc. All rights reserved.

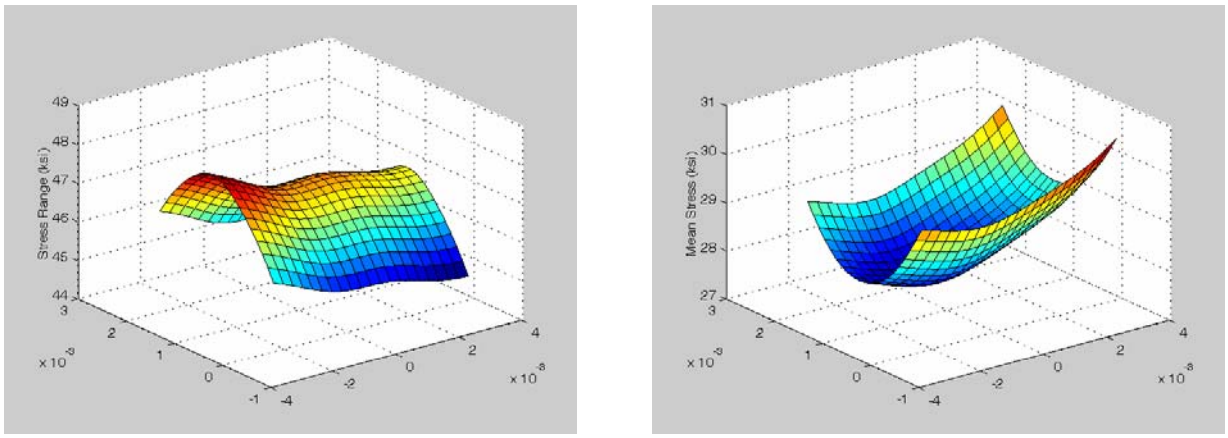

Stress Range at L7 of Hole 3 Mean Stress at L7 of Hole 3

Figure 8. Conditional 2D Response Surface for Hole 3 Location 7

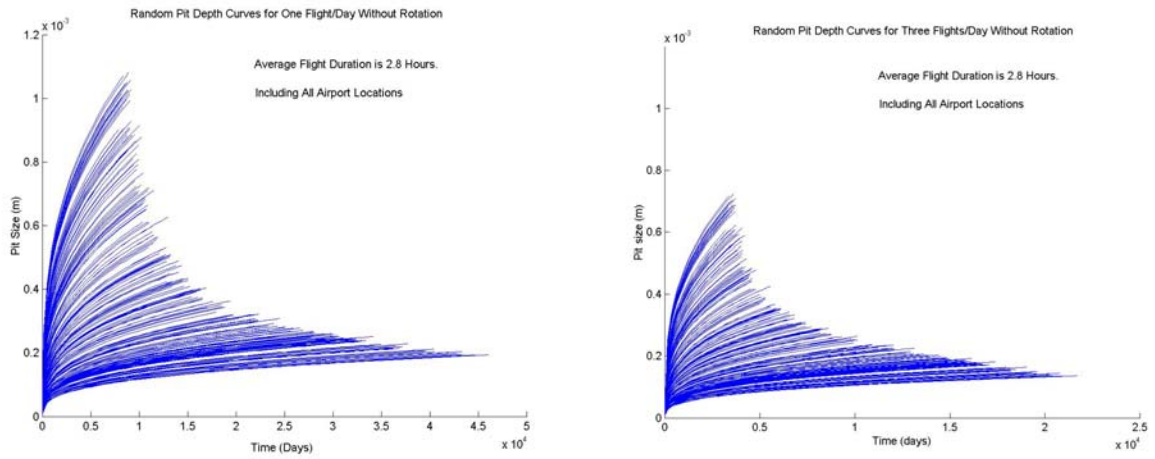

Figure 9. Simulated Pit Growth Curves for Without Airport Rotation

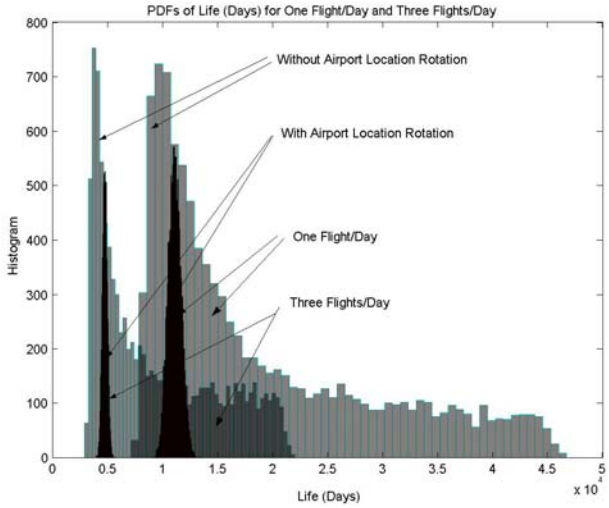

Figure 10. Corrosion-Fatigue Statistical Histograms for the Four Scenarios

Copyright 2005 by the American Institute of Aeronautics and Astronautics, Inc. All rights reserved.

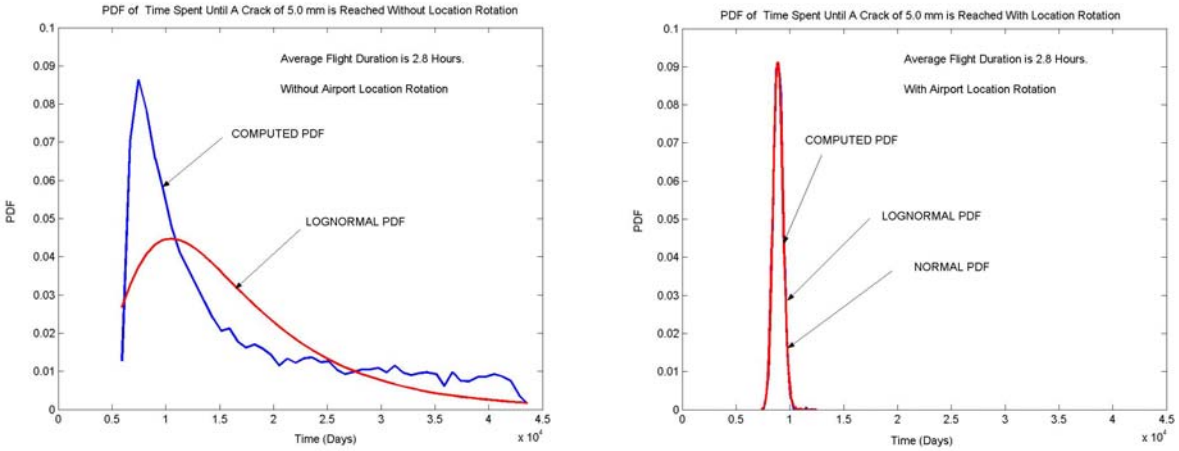

Figure 11. PDF of CF Life for One-Flight/Day Without and With Airport Rotation

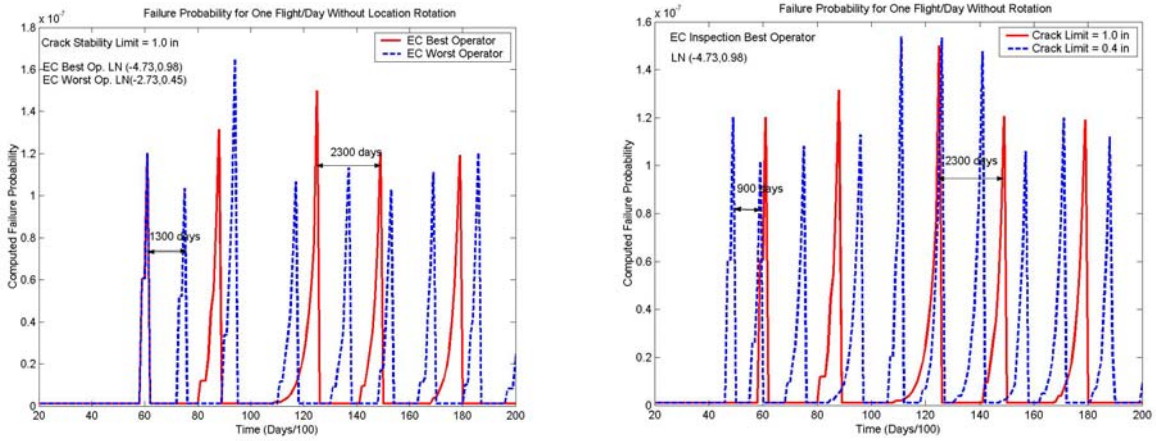

Figure 12. Risk-based Inspection Times for One-Flight/Day, Without Rotation and Given Target Risk of $2x10^{-7}$: a) Effect of the Operator's Skill and b) Effect of Crack Limit Criterion.

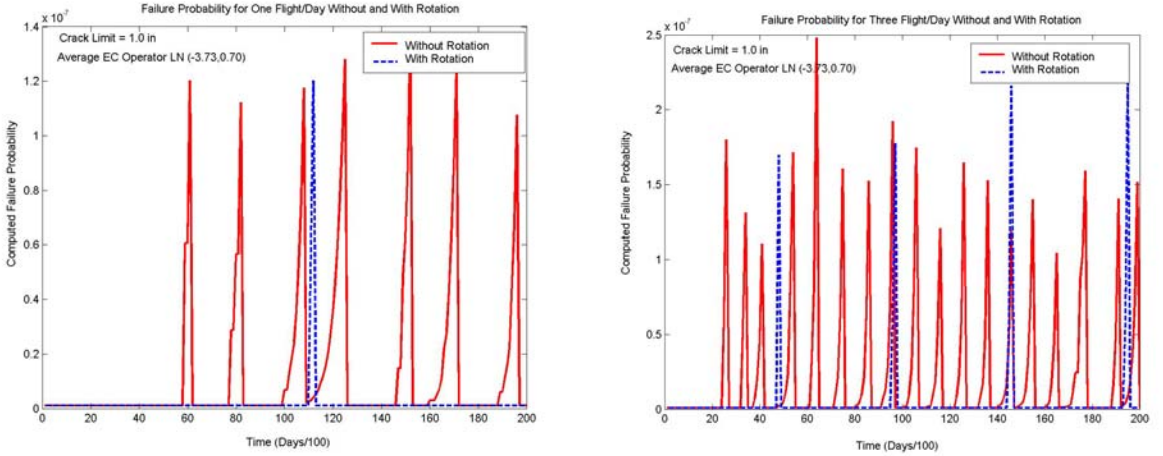

Figure 13. Risk-based Inspection Times Without & With Rotation for A Given Target Risk; a) One Flight/Day and b) Three Flights/Day

Copyright 2005 by the American Institute of Aeronautics and Astronautics, Inc. All rights reserved.